Nuclear Forward Scattering of Synchrotron Radiation in Pulsed High Magnetic Fields

C. Strohm,* P. Van der Linden, and R. Rüffer

European Synchrotron Radiation Facility, BP220, 38043 Grenoble, France

(Received 10 August 2009; published 24 February 2010; publisher error corrected 13 April 2010)

We report the demonstration of nuclear forward scattering of synchrotron radiation from ^{57}Fe in ferromagnetic α iron in pulsed high magnetic fields up to 30 T. The observed magnetic hyperfine field follows the calculated high field bulk magnetization within 1%, establishing the technique as a precise tool for the study of magnetic solids in very high magnetic fields. To perform these experiments in pulsed fields, we have developed a detection scheme for fully time resolved nuclear forward scattering applicable to other pump probe experiments.

DOI: 10.1103/PhysRevLett.104.087601 PACS numbers: 76.80.+y, 75.50.Bb, 76.60.Jx

Nuclear forward scattering (NFS) of synchrotron radiation being a time analog of the classical Mössbauer effect (ME) provides a unique tool for the study of the structure, valence, magnetism, and dynamics through a local probe, and both techniques are used extensively for the study of magnetic solids [1]. Synchrotron techniques using hard x rays are well suited to perform experiments under extreme conditions in general and, in particular, under high magnetic fields. Pulsed magnets are an economic and flexible choice to generate high fields beyond the limits of current superconducting and resistive magnet technology in the laboratory [2]. Combining both technologies, various synchrotron methods such as powder diffraction [3,4], single crystal diffraction [5], x-ray absorption spectroscopy [6], and x-ray magnetic circular dichroism [7] have already been developed in pulsed high fields. NFS and ME experiments, however, were up to now limited to superconducting magnets. Here we report the first demonstration of NFS in pulsed fields. To illustrate the precision of the present experiment we compare the magnetic hyperfine interactions (HFI) in ferromagnetic α iron with the bulk magnetization up to 30 T. As NFS is intrinsically a time resolved method, where photons scattered by the nuclei are separated in time from the transmitted beam and from electronic scattering, we have developed a detection scheme based on recording the full time information for each event in order to perform NFS in time varying fields.

Soon after the first observation of the ME from the 14.413 keV $1/2 \rightarrow 3/2$ $M1$ transition of ^{57}Fe [8,9], it was shown that the magnetic hyperfine field in ferromagnetic α iron is directed parallel [10] and opposite [11] to the magnetization. The ground and the excited state are split into 2 and 4 sublevels through the interaction of the nuclear magnetic moments with the internal magnetic field, Fig. 1(a). This nuclear Zeeman effect leads to the observation of up to six transitions [11]. Fe has the electronic configuration $[\mathrm{Ar}]3d^6 4s^2$, and the magnetic hyperfine field is originated through the polarization of the core s electrons through the incomplete $3d$ shell, the conduction electron polarization, and the field due to the orbital momentum of the $3d$ electrons. The size of the different contributions and the resultant magnetic hyperfine field have been calculated by several groups [12–15] and some of the contributions were measured individually [16,17]. Although the temperature dependence of H_{HFI} closely follows the temperature dependence of the bulk magnetization [18,19], a small deviation is systematically observed when plotting both over a large temperature range. Two classes of explanations were proposed to account for this apparent temperature dependence of the hyperfine coupling: (i) an intrinsic variation of the hyperfine coupling and (ii) differences in the domain and wall hyperfine fields. Only recently the discrepancy was rationalized with the latter, based on precise measurements and thermodynamic considerations [20]. However, once technical saturation is reached in an applied field, the hyperfine field is expected to be determined by the intrinsic coupling of its contributions to the local and itinerant moments only. Similar to the temperature dependence, a precise comparison of the experimental values for H_{HFI} with the values for the bulk magnetization over a broad field range provides a test of both the balance between the different contributions to the hyperfine field in ferromagnetic α-Fe and the precision of the method. In the present demonstration experiment we measured the total field H_n at the ^{57}Fe nuclei in a sample of ferromagnetic α Fe up to 30 T, further than any previous ME or NFS experiment known to us.

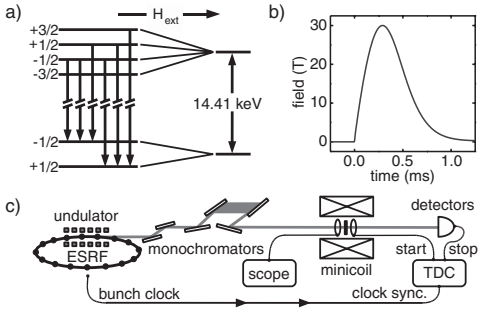

FIG. 1. (a) Nuclear level scheme for the for the 14.413 keV Mössbauer transition of ^{57}Fe in α Fe. (b) Magnetic field pulse. (c) Experiment.

Contrary to the classical ME, where a narrow band (^{57}Fe, 4.7 neV) source is scanned across the transitions shown in Fig. 1(a), they are excited simultaneously with short pulses (100 ps) of coherent broadband radiation (2.5 meV) from isolated single bunches in the case of NFS. In the subsequent γ decay this leads to interference between the respective transition frequencies from the levels split through hyperfine interactions. The quanta from the decay are detected in the empty time window of 176 ns between the bunches in 16 bunch mode operation of the European Synchrotron Radiation Facility (ESRF). In the usual detection scheme [21], the NFS time spectra revealing the interference pattern are obtained through histograming of the events as a function of their delay with respect to the last exciting prompt pulse, abandoning the information on the absolute time of detection. Parameters determining the hyperfine interactions and the optical properties of the sample, like an applied magnetic field, are therefore required to remain constant during the acquisition of the time spectrum. A separate spectrum is acquired for each set of parameters. The same detection scheme is also applicable to pump probe experiments in the opposite extreme, when the parameters change on a time scale which is very short compared to the lifetime of the nuclear transition. In this case, the temporal evolution of the parameter leads to a change within the time spectra [22].

In order to record NFS in fields varying on the millisecond time scale, one has to perform photon count statistics in two dimensions: first, as a function of time with respect to the exciting prompt pulse and, second, as a function of the time varying magnetic field. We therefore have developed a detection scheme for the third intermediate regime, where the parameters vary on a time scale (1 ms) which is long compared to the lifetime of the nuclear transition (^{57}Fe, $\tau_0 = 141$ ns), but very short compared to the time necessary to acquire time spectra (seconds). Our detection scheme is based on recording the full time information for each count and allows one to exploit the entire duration of the magnetic field pulses.

The shape of the field pulses, shown in Fig. 1(b), is obtained through integration of the signal of a pickup coil, recorded by an oscilloscope. Simultaneously, the transmitted and forward-scattered photons are registered with a time to digital converter (TDC) [23] in single-sweep, multistop mode, using the same trigger as the field signal for a precise synchronization of both the oscilloscope and the TDC, Fig. 1(c). This allows one to assign a magnetic field value to each event through temporal correlation of the two recordings for each pulse. There is no correlation between the field trigger and the bunch timing in the storage ring, and prompt and delayed events cannot be distinguished in the TDC data stream. In order to determine the delay of each event with respect to the last exciting pulse of prompt radiation, we therefore make use of the strict periodicity and the higher probability of prompt events: For each field pulse, we calculate the histogram $A_k = \sum_{i\mathrm{mod}(T_b/\Delta t)=k} a_i$, $k = 0 \ldots T_b/\Delta t$ over the binary data stream $a_i \in \{0, 1\}$, $i = 0 \ldots T/\Delta t$ from the TDC, where T is the total length of the recording, T_b is the bunch spacing, and Δt is the temporal bin width. In the resulting histogram, the temporal position of the prompt radiation is marked by a maximum $\max(A_k)$ at $k_{\max}$. The delay for an event in the ith bin is then calculated as $t_i = [i\mathrm{mod}(T_b/\Delta t) - k_{\max}]\Delta t$ for $i \geq k_{\max}$ and $t_i + T_b$ for $i < k_{\max}$. For the evaluation, we exploit the full time information for each event on three different scales: (a) the time of the common trigger allows a full replay of the experiment after completion, (b) the time of detection after the common trigger is used to assign the magnetic field value to each count, and (c) the delay with respect to the last prompt pulse allows one to extract the time spectra through binning in time and field.

As NFS is a flux-limited method, it is necessary to average over thousands of field pulses in order to record exploitable time spectra. A crucial point was therefore the development of a liquid nitrogen cooled high duty cycle minicoil with internal cooling [24]. The coil reaches repetition rates of 6 min^{-1} at a total pulse length of 1 ms and 30 T peak field.

For the sample, a disk with a diameter of 1 mm was laser cut from a 10 μm thick polycrystalline foil of ferromagnetic α Fe with an enrichment of 90% in the Mössbauer isotope ^{57}Fe. The disk was glued to a diamond substrate with 155 μm thickness [Fig. 4(a) inset] and mounted in the gas flow of the He sample cryostat. The magnetic field is oriented along the beam, and perpendicular to the surface of the foil. The setup at the beam line ID18 at the ESRF is shown schematically in Fig. 1(c). The sample was irradiated with a monochromatic beam with a bandwidth of 2.5 meV, which is large compared to the nuclear level splitting (300 neV), and the transmitted photons were counted with a stack of four avalanche photodiodes. The average zero field count rate was about 25 kHz in the time window from 12 to 173 ns, and a total of 65 769 counts were recorded in 2131 field pulses during 9 h, 40 min.

Figure 2(a) shows a simulation of the NFS intensity and Fig. 2(b) shows all experimentally recorded events in the H-t plane. The data are continuous in the H-t plane and allow for different binning after the experiment. The simultaneous acquisition guarantees excellent consistency of the data over the whole field range. The NFS intensity is determined by two contributions: an aperiodic beat that reflects the effective thickness of the sample and a periodic quantum beat with a period inversely proportional to the magnetic field at the nucleus. Once the sample is fully magnetized only the $\Delta m = \pm 1$ transitions are excited for $\mathbf{H} \parallel \mathbf{k}$, leading to the observation of one quantum beat frequency due to the energy difference $\Delta E = (\mu_g/I_g - \mu_e/I_e)\mu_0 H_n$. In order to extract the NFS time spectra shown in Fig. 3, events taken in rising and falling field were summed together over field regions of 2 T. With the available statistics we could not find a significant difference when tentatively summing spectra taken in the rising

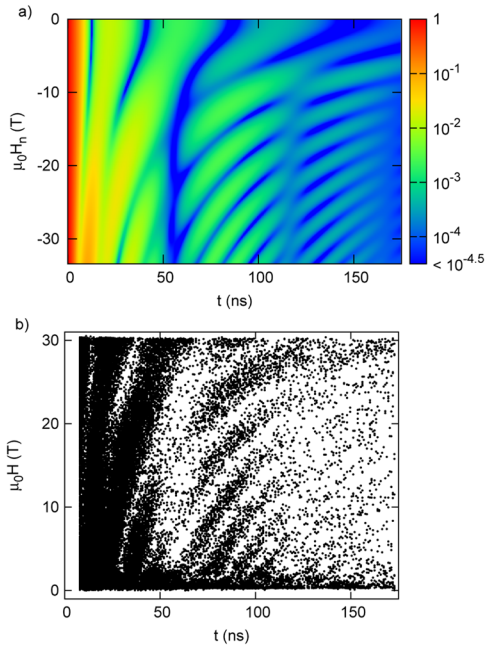

FIG. 2 (color online). NFS in pulsed high magnetic fields from a 10 μm thick, polycrystalline foil of ferromagnetic α Fe. (a) Simulation of the NFS intensity as a function of delay and the field at the nucleus for a Lamb-Mössbauer factor of 0.82. (b) Experimentally observed events as a function of delay and the applied field. Note the different vertical scales and ranges.

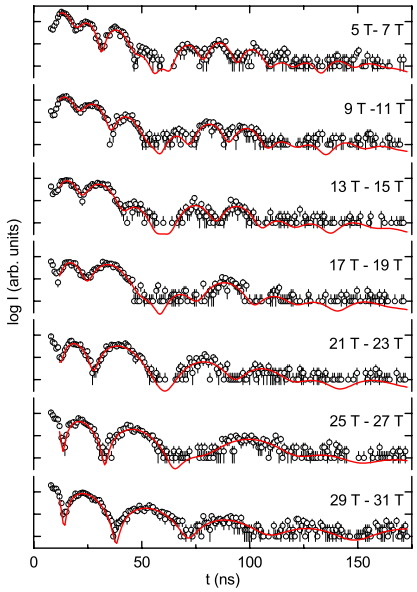

FIG. 3 (color online). Selected time spectra. Nuclear forward scattering intensity as a function of time with respect to the last prompt pulse. The spectra were extracted from Fig. 2 through binning in time (0.8 ns) and field (2 T). Points, data with statistical error; line, fit to the data.

and falling parts of the pulse separately. The time spectra in Fig. 3 were fitted in the range from 12 to 173 ns using the MOTIF package [25] with the Lamb-Mössbauer factor and H_n as free parameters. In this fit, the averaging over the field regions was approximated with an incoherent Gaussian distribution. The Lamb-Mössbauer factors obtained from the fits do not show a significant field dependence. Their average of 0.82(1) corresponds to a sample temperature of 214(22) K according to [26], even though the cryostat was operated at 15 K during the whole experiment. Heating the sample to this temperature requires an energy of 2.4×10^{-3} J, whereas a conservative estimate for the total energy generated due to eddy current heating through the whole pulse remains 1 order of magnitude below this value. With a demagnetization factor of $N = 1$, in-plane orientation of the moments is more favorable in the absence of an external field. We therefore believe that the heating is mainly due to magnetization losses until technical saturation is reached. The field at the nucleus $H_n = H_{\mathrm{HFI}}(T, H_i) + H_i$ that is observed in the experiment is the sum of the field $H_{\mathrm{HFI}}(T, H_i)$ due to the hyperfine coupling to the local and itinerant moments and the internal field $H_i = H_{\mathrm{ext}} - H_D + H_L$, where H_{ext}, $H_D = NM(T, H_i)$, and H_L are the external, the demagnetizing, and the Lorentz fields, N is the demagnetization factor, and $M(T, H_i)$ is the bulk magnetization. Figure 4(a) shows H_n and the corresponding ΔE as a function of the applied field. The points are the values obtained from a fit of the time spectra in Fig. 3 and the line represents a calculation of H_n.

As H_{HFI} in ferromagnetic α ^{57}Fe is opposite to the atomic magnetic moment, H_n is first reduced by the applied field and eventually changes sign when the external field compensates the hyperfine field plus the demagnetizing and the Lorentz fields. We may rewrite the above expression as $H_n(T, H_i) - H_{\mathrm{ext}} = H_{\mathrm{HFI}}(T, H_i) - NM(T, H_i) + H_L$ in order to separate the quantities measured in the present experiment (left side) from values to be calculated or to be taken from the literature (right side). In Fig. 4(b) we plot the experimental points along with the calculation using values from [20,27] without adjustable parameters. At the temperature of the experiment, the temperature dependence of the magnetization is well described by spin waves. The external field is included through a magnetic gap temperature and an additional linear term to account for the Pauli susceptibility of the electron gas. The line was calculated assuming a direct proportionality between H_{HFI} and the total moment per unit mass. The comparison shows that the magnetic hyperfine field follows the bulk magnetization without a significant field dependence of the hyperfine coupling within the experimental accuracy of about 1% and illustrates the accuracy of the measurement. The systematic shift lies within the uncertainty of the input values and temperature determination, but we would like to point out that systematic errors in the field measurement and in the fit of the time spectra are at least of the same order.

In conclusion, we have demonstrated NFS in pulsed high magnetic fields up to 30 T in a polycrystalline foil of ferromagnetic α iron. The magnetic hyperfine field is compensated by the applied field and follows the field dependent bulk magnetization within the accuracy of the

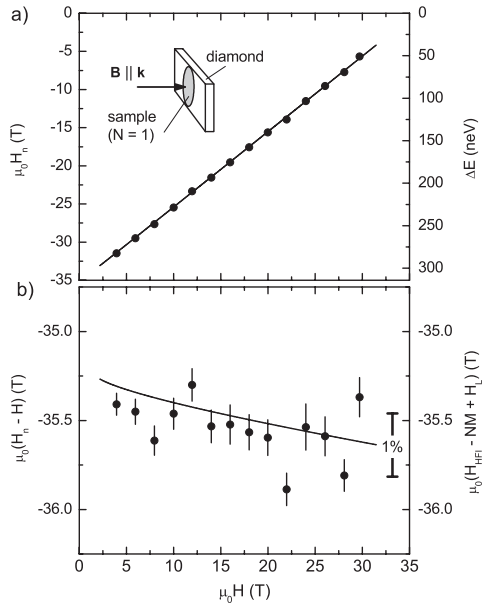

FIG. 4. (a) Field at the ^{57}Fe nuclei and energy difference ΔE as a function of the applied magnetic field. The points were obtained by fitting the time spectra in Fig. 3. Line: Calculated internal field. Inset: Sample geometry. (b) Points, left label: Measured field at the ^{57}Fe nuclei minus the applied field. Error bars: Fitting error. Line, right label: Calculation of the magnetic hyperfine field minus the demagnetizing field.

experiment. The results suggest field independent hyperfine coupling constants. As NFS is intrinsically a time resolved method, we have developed a detection scheme to perform truly time dependent NFS in the domain where the hyperfine interactions vary slowly with respect to the lifetime, but very fast compared to the acquisition time in order to record NFS time spectra in fields varying on the millisecond scale. The detection scheme exploits the full magnetic field pulse duration, and the data are continuous in the magnetic field and allow for different binning after completion of the experiment. The use of this detection scheme is not limited to experiments in pulsed magnetic fields and allows us to perform pump probe experiments with NFS in general. Contrary to classical Mössbauer spectroscopy, which needs to address the issues of source splitting or magnetic shielding of the source, the present method can be used in even higher pulsed fields without modification in the future. NFS in pulsed fields is not restricted to ^{57}Fe and can be performed with Mössbauer isotopes for which NFS has been developed with sufficient flux. ^{149}Sm, ^{151}Eu, ^{161}Dy, and ^{61}Ni are of particular interest for the study of magnetic solids. For the future, NFS in pulsed fields opens a wide range of opportunities, ranging from the study of molecular magnets, spin crossover systems, mixed valence compounds, Fe-garnet ferrimagnets, over frustrated magnets to Fe-pnictide superconductors. Subjects of interest include magnetization steps in "Fe_6," "Fe_{10}," and "Fe_{12}," the canted phases of $Yb_3Fe_5O_{12}$ and $Er_3Fe_5O_{12}$, or the triangular lattice antiferromagnets like $RbFe(MoO_4)_2$, $KFe(MoO_4)_2$, and $CuFeO_2$. For the latter we anticipate, for example, the possibility to directly observe the different metamagnetic phases in the *B-t* plane and to study the spin structure after appropriate binning of the data.

The authors would like to acknowledge the help of A. I. Chumakov and T. Roth at the beam line, T. H. Deschaux Beaume Dang for the fast summing discriminator, J. Härtwig for the diamonds, and W. Wagner from Fast Comtec.

*cornelius.strohm@esrf.fr

[1] E. Gerdau and H. de Waard, Hyperfine Interact. **123-124** (1999).
[2] F. Herlach, Rep. Prog. Phys. **62**, 859 (1999).
[3] Y. Narumi *et al.*, J. Synchrotron Radiat. **13**, 271 (2006).
[4] P. Frings *et al.*, Rev. Sci. Instrum. **77**, 063903 (2006).
[5] Y. H. Matsuda *et al.*, J. Phys. Soc. Jpn. **75**, 024710 (2006).
[6] Y. H. Matsuda *et al.*, J. Phys. Soc. Jpn. **76**, 034702 (2007).
[7] O. Mathon *et al.*, J. Synchrotron Radiat. **14**, 409 (2007).
[8] R. V. Pound and G. A. Rebka, Phys. Rev. Lett. **3**, 554 (1959).
[9] J. P. Schiffer and W. Marshall, Phys. Rev. Lett. **3**, 556 (1959).
[10] G. J. Perlow *et al.*, Phys. Rev. Lett. **4**, 74 (1960).
[11] S. S. Hanna *et al.*, Phys. Rev. Lett. **4**, 513 (1960).
[12] R. E. Watson and A. J. Freeman, Phys. Rev. **123**, 2027 (1961).
[13] S. Wakoh and J. Yamashita, J. Phys. Soc. Jpn. **25**, 1272 (1968).
[14] K. J. Duff and T. P. Das, Phys. Rev. B **12**, 3870 (1975).
[15] T. P. Das, Phys. Scr. **11**, 121 (1975).
[16] C. Song, J. Trooster, and N. Benczer-Koller, Phys. Rev. B **9**, 3854 (1974).
[17] P. C. Riedi, J. Phys. F **5**, 2191 (1975).
[18] D. E. Nagle *et al.*, Phys. Rev. Lett. **5**, 364 (1960).
[19] R. S. Preston, S. S. Hanna, and J. Heberle, Phys. Rev. **128**, 2207 (1962).
[20] U. Köbler *et al.*, Physica (Amsterdam) **339B**, 156 (2003).
[21] A. Q. R. Baron, Hyperfine Interact. **125**, 29 (2000).
[22] Yu. V. Shvydko *et al.*, Phys. Rev. Lett. **77**, 3232 (1996).
[23] FAST ComTec, Multiscaler P7889, http://www.fastcomtec.com
[24] P. E. J. M. van der Linden *et al.*, Rev. Sci. Instrum. **79**, 075104 (2008).
[25] Yu. V. Shvyd'ko, Hyperfine Interact. **125**, 173 (2000).
[26] U. Bergmann *et al.*, Phys. Rev. B **50**, 5957 (1994).
[27] R. Pauthenet, *High Field Magnetization in Magnetic Materials* (North-Holland, Amsterdam, 1983), p. 77.